Intramolecular Spin Interactions in Bis(phenoxyl)metal Complexes of Zinc(II) and Copper(II)

Eckhard Bill,* Jochen Müller, Thomas Weyhermüller, and Karl Wieghardt*

Max-Planck-Institut für Strahlenchemie, D-45470 Mülheim an der Ruhr, Germany

Received April 12, 1999

The pendent arm macrocyclic ligand 1-ethyl-4,7-bis(3-*tert*-butyl-5-methoxy-2-hydroxybenzyl)-1,4,7-triazacyclononane, H_2L, forms stable complexes in methanol with zinc(II) and copper(II) ions: $[Zn^{II}(L)]\cdot H_2O$ (**1**); $[Cu^{II}(L)]\cdot 0.5\ CH_2Cl_2$ (**2**); $[Cu^{II}(LH)](ClO_4)$ (**3**). The crystal structures of **1** and **2** have been determined by X-ray crystallography: **1** crystallizes in the orthorhombic space group *Pbca* with $a = 21.100(4)$ Å, $b = 10.267(2)$ Å, $c = 28.896(6)$ Å, $V = 6260(2)$ Å^3, $Z = 8$; **2** crystallizes in the monoclinic space group *C*2/*c* with $a = 14.447(2)$ Å, $b = 25.522(4)$ Å, $c = 17.296(3)$ Å, $V = 6300(2)$ Å^3, $Z = 8$. In CH_2Cl_2 solution complexes **1** and **2** can electrochemically be reversibly oxidized by two successive one-electron processes generating the stable phenoxyl mono- ($[\mathbf{1}]^{\bullet+}$; $[\mathbf{2}]^{\bullet+}$) and diradicals ($[\mathbf{1}]^{2\bullet2+}$, $[\mathbf{2}]^{2\bullet2+}$). In contrast, **3** containing a coordinated phenol and one phenolate can only be oxidized to the monoradical $[\mathbf{3}]^{\bullet2+}$. The electronic structure of these mono- and diradicals have been established by UV/vis and EPR spectroscopy in fluid and/or frozen solution. All oxidations are ligand-centered generating coordinated phenoxyl radicals. In $[\mathbf{1}]^{2\bullet2+}$ the two unpaired electrons interact with each other via exchange and weak dipolar couplings of the order of -3 and 10^{-2} cm^{-1}, respectively. The monoradicals $[\mathbf{2}]^{\bullet+}$ and $[\mathbf{3}]^{\bullet2+}$ are nearly EPR-silent; an $S_t = 1$ excited state for both species is barely observable due to large zero-field splitting. In $[\mathbf{1}]^{\bullet+}$ the phenoxyl radical electron is localized on one phenyl ring whereas for $[\mathbf{2}]^{\bullet+}$ some degree of delocalization over both phenyl rings may be present. The diradical $[\mathbf{1}]^{2\bullet2+}$ possesses a diamagnetic whereas $[\mathbf{2}]^{2\bullet2+}$ has an $S_t = {}^3/_2$ ground state.

Introduction

In the past few years a rapidly growing number of phenoxyl radical complexes of the first-row transition metals have been synthesized with a strong emphasis on species containing copper(II) ions.[1−8] This interest has been fueled by the discovery that two enzymes, namely galactose oxidase[9] and glyoxal oxidase,[10] have active sites composed of a single Cu^{II} and a coordinated tyrosyl radical. The electronic structure of such phenoxylcopper(II) complexes is rather interesting because the two unpaired electrons of the Cu^{II} (d^9, $S_{Cu} = {}^1/_2$) and of the coordinated phenoxyl ($S_{rad} = {}^1/_2$) are intramolecularly anti- or ferromagnetically coupled yielding an $S_t = 0$ or $S_t = 1$ ground state.

Recently, we have analyzed this phenomenon within the frame of the Goodenough−Kanomori rules for exchange coupling.[11] In five-coordinate square-based pyramidal and Jahn−Teller distorted octahedral Cu^{II} complexes the metal-centered magnetic orbital is often a $d_{x^2-y^2}$ orbital whereas the magnetic orbital of a phenoxyl radical is of π-type. The sign of the exchange coupling constant is then determined by two parameters: (i) the $Cu^{II}-O-C_{phenyl}$ bond angle α and (ii) the dihedral angle β defined by the *x*,*y*-plane at the Cu^{II} ion and the phenyl ring of the organic radical. If $\alpha = 180°$ the coupling is always ferromagnetic in nature irrespective of β due to the orthogonality of the magnetic orbitals. On the other hand, at $\alpha \sim 130°$ the dihedral angle β determines the ground state of the phenoxylcopper(II) complex: it is $S_t = 0$ at β values between $\sim$25−90°, and $S_t = 1$ is observed if β is close to zero (Scheme 1).

In this paper we describe two complexes which contain *two* coordinated phenoxyl ligands in cis position relative to each other and investigate their electronic structures by using EPR spectroscopy. Similar species have recently been reported by Tolman et al.[1] The spin interactions in these bis(phenoxyl)metal complexes are found to be different from those reported for analogous bis(semiquinonato)metal complexes.[12−14]

(1) Halfen, J. A.; Jazdzewski, B. A.; Mahapatra, S.; Berreau, L. M.; Wilkinson, E. C.; Que, L.; Tolman, W. B. *J. Am. Chem. Soc.* **1997**, *119*, 8217.
(2) Halfen, J. A.; Young, V. G.; Tolman, W. B. *Angew. Chem.* **1996**, *108*, 1832; *Angew. Chem., Int. Ed. Engl.* **1996**, *35*, 1687.
(3) Sokolowski, A.; Leutbecher, H.; Weyhermüller, T.; Schnepf, R.; Bothe, E.; Bill, E.; Hildebrandt, P.; Wieghardt, K. *J. Biol. Inorg. Chem.* **1997**, *2*, 444.
(4) Wang, Y.; Stack, T. D. P. *J. Am. Chem. Soc.* **1996**, *118*, 13097.
(5) Zurita, D.; Gautier-Luneau, I.; Menage, S.; Pierre, J.-L.; Saint-Aman, E. *J. Biol. Inorg. Chem.* **1997**, *2*, 46.
(6) Zurita, D.; Scheer, C.; Pierre, J.-L.; Saint-Aman, E. *J. Chem. Soc., Dalton Trans.* **1996**, 4331.
(7) Itoh, S.; Takayama, S.; Arakawa, R.; Furuta, A.; Komatsu, M.; Ishida, A.; Takamuku, S.; Fukuzumi, S. *Inorg. Chem.* **1997**, *36*, 1407.
(8) Halcrow, M. A.; Chia, L. M. L.; Liu, X.; McInnes, E. J.; Yellowlees, L. J.; Mabbs, F. E.; Davies, J. E. *Chem. Commun.* **1998**, 2465.
(9) (a) Whittaker, J. W. In *Metalloenzymes Involving Amino Acid Residue and Related Radicals*; Sigel, H., Sigel, A., Eds.; Marcel Dekker: New York, 1994; Vol. 30, pp 315−360. (b) Knowles, P. F.; Ito, N. *Perspectives in Bio-inorganic Chemistry*; Jai Press Ltd.: London, 1994; Vol. 2, pp 207−244.
(10) Whittaker, M. M.; Kersten, P. J.; Nakamura, N.; Sanders-Loehr, J.; Schweizer, E. S.; Whittaker, J. W. *J. Biol. Chem.* **1996**, *271*, 681.
(11) Müller, J.; Weyhermüller, T.; Bill, E.; Hildebrandt, P.; Ould-Moussa, L.; Glaser, T.; Wieghardt, K. *Angew. Chem., Int. Ed. Engl.* **1998**, *37*, 616.
(12) Prokofev, A. I.; Malysheva, N. A.; Busnov, N. N.; Solodovnikov, S. P.; Kabachnik, M. I. *Dokl. Akad. Nauk SSR* **1980**, *252*, 236.

10.1021/ic990396j CCC: $18.00
Published on Web 11/18/1999

Scheme 1. Relative Orientations of the Magnetic Orbitals $d_{x^2-y^2}$ of the Cu^{II} Ion in a Square-based Pyramidal Ligand Environment and the π-orbital of a Phenoxyl Radical[a]

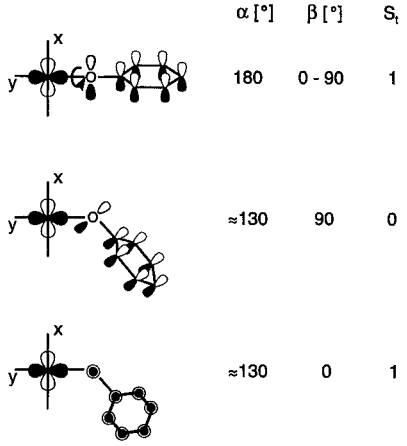

[a] α (deg) represents the Cu−O−C bond angle, and β (deg) is the dihedral angle between the *x*,*y*-plane at Cu^{II} and the phenyl ring. S_t is the expected ground state of the Cu^{II}−phenoxyl species.

Results

The ligand 1-ethyl-4,7-bis(3-*tert*-butyl-5-methoxy-2-hydroxybenzyl)-1,4,7-triazacyclononane, H_2L, has been prepared from

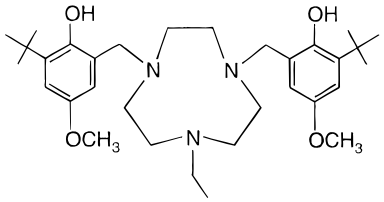

H_2L

the reaction of 1-ethyl-1,4,7-triazacyclononane, paraformaldehyde, and 2-*tert*-butyl-4-methoxyphenol in methanol.

The reaction of H_2L with 1 equiv of $Zn(BF_4)_2 \cdot 4H_2O$ or CuCl (in the presence of air) and 3 equiv of $K[OC(CH_3)_3]$ in methanol produced colorless crystals of $[Zn^{II}(L)] \cdot H_2O$ (**1**) and green-brown $[Cu^{II}(L)] \cdot 0.5CH_2Cl_2$ (**2**) (upon addition of CH_2Cl_2 to the solution), respectively. Addition of $HClO_4$ to the above copper containing solution initiated the precipitation of violet $[Cu^{II}(LH)](ClO_4)$ (**3**).

Figure 1 shows the structures of the neutral molecules in crystals of **1** and **2**, and Table 1 gives selected bond distances and angles. The Zn^{II} and Cu^{II} ions are coordinated by the pentadentate dianion L^{2-}, respectively, in a distorted square-based pyramidal fashion where the phenolate oxygen atoms occupy two equatorial sites in cis position relative to each other and two cis-amine nitrogen atoms are in the other two sites; the third amine nitrogen is the apical position.

Both structures show interesting packing effects in the solid state. In **1** a water molecule of crystallization forms two O−H···O bonding contacts to one phenolate oxygen atom (O2) and a methoxy oxygen atom of a neighboring molecule (O3B). The distances O2···O5 and O5···O3B are at 2.789 and 3.022 Å. This renders the two $Zn-O_{phenolate}$ bonds of a neutral molecule different. In **2** two neutral molecules $[Cu^{II}(L)]$ are packed pairwise in such a fashion that the two equatorial cis-O_2N_2 planes of the square-based pyramidal polyhedra face each other. The phenolate oxygen atom O1 occupies the vacant sixths coordination site of the second molecule (O1a···Cu1b 4.422 Å). Again the two $Cu-O_{phenolate}$ bonds are different.

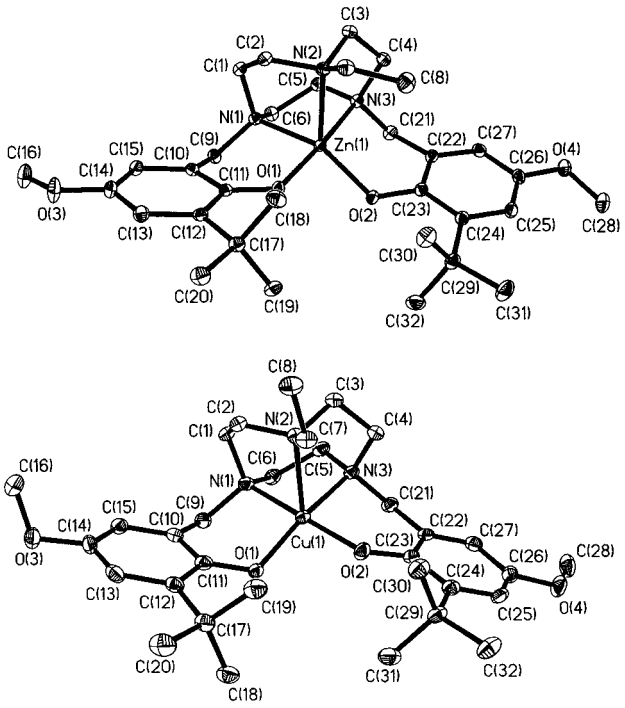

Figure 1. Perspective view of the neutral molecules in (a) crystals of **1** and (b) crystals of **2**. The thermal ellipsoids are drawn at the 40% probability level.

Table 1. Selected Bond Distances (Å) and Angles (deg)

	complex	
	1 (M = Zn)	**2** (M = Cu)
M−O1	1.963(1)	1.936(2)
M−O2	1.934(1)	1.889(2)
M−N1	2.113(1)	2.941(2)
M−N2	2.156(1)	2.357(2)
M−N3	2.277(1)	2.055(2)
O1−C11	1.328(2)	1.331(3)
O2−C23	1.340(2)	1.330(3)
O3−C14	1.391(2)	1.402(3)
O3−C16	1.430(2)	1.415(3)
O4−C26	1.391(2)	1.393(3)
O4−C28	1.417(2)	1.424(3)
O2−M−O1	93.22(4)	89.28(7)
O2−M−N1	140.41(5)	173.25(8)
O1−M−N1	92.62(5)	93.37(8)
O2−M−N2	130.42(5)	102.90(7)
O1−M−N2	103.81(5)	110.49(7)
N1−M−N2	85.62(5)	81.98(8)
O2−M−N3	89.27(4)	90.61(8)
O1−M−N3	172.11(4)	167.97(8)
N1−M−N3	80.75(5)	85.50(8)
N2−M−N3	80.08(5)	81.24(8)
C11−O1−M	129.98(9)	123.4(2)
C23−O2−M	127.23(9)	130.4(2)

In contrast, the ^1H NMR spectrum of **1** in $CDCl_3$ solution clearly shows that the two six-membered chelate rings, $\overline{Zn-O-C-C-C-N}$, are equivalent and conformatively rigid because the two diastereotopic benzylic protons of both benzyl groups give rise to only two doublets (see Experimental Section).

Cyclic and square-wave voltammograms of complexes have

(13) Lange, C. W.; Couklin, B. J.; Pierpont, C. G. *Inorg. Chem.* **1994**, *33*, 1276.
(14) Ozarowski, A.; McGarvey, B. R.; Peppe, C.; Tuck, D. G. *J. Am. Chem. Soc.* **1991**, *113*, 3288.

Table 2. Redox Potentials of Complexes[a]

complex	$E_{1/2}$, V vs Fc^+/Fc	
1	+0.15	−0.10
2	+0.14	−0.10
3	+0.14	

[a] Conditions: CH_2Cl_2 solvent containing 0.10 M $[TBA]PF_6$; glassy carbon working electrode; scan rate 200 mV s^{-1}.

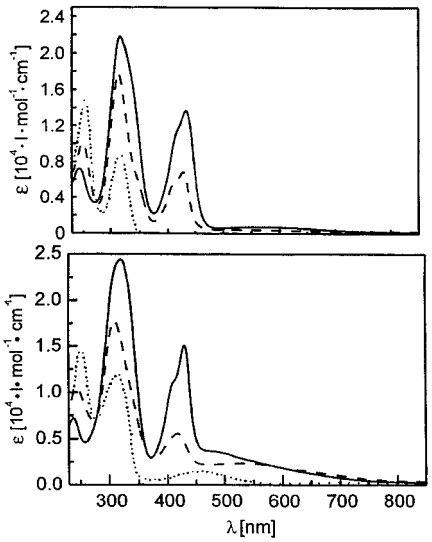

Figure 2. Top: Electronic spectra of **1** (···) and their electrochemically generated oxidized forms $[\mathbf{1}]^{\bullet+}$ (- - -) and $[\mathbf{1}]^{2\bullet2+}$ (—) in CH_2Cl_2 solution (0.10 M $[TBA]PF_6$) at 298 K. Bottom: Electronic spectra of **2** (···) and their electrochemically generated oxidized forms $[\mathbf{2}]^{\bullet+}$ (- - -) and $[\mathbf{2}]^{2\bullet2+}$ (—) in CH_2Cl_2 solution (0.10 M $[TBA]PF_6$) at 298 K.

been recorded in CH_2Cl_2 solution containing 0.10 M $[TBA]PF_6$ as supporting electrolyte at a glassy carbon working electrode. Ferrocene was used as internal standard; all potentials are referenced vs the ferrocenium/ferrocene (Fc^+/Fc) couple. The results are summarized in Table 2.

Both **1** and **2** display in the potential range +0.5 to −1.7 V two reversible one-electron oxidation waves which are ligand-centered processes corresponding to two successive one-electron oxidations of a coordinated phenolate to a phenoxyl ligand (eq 1).

$$[M^{II}(L)]^0 \underset{+e}{\overset{-e}{\rightleftharpoons}} [M^{II}(L)]^{\bullet+} \underset{+e}{\overset{-e}{\rightleftharpoons}} [M^{II}(L)]^{2\bullet2+} \quad M = Zn, Cu \tag{1}$$

In contrast, **3** displays only a single reversible, ligand-centered one-electron oxidation wave. We take this as evidence that protonation of **2** at a coordinated phenolate yielding a coordinated phenol in **3** has taken place. In the potential range employed we did not observe metal-centered reductions of the Cu^{II} ions in **2** and **3**. Coulometric oxidations at appropriately fixed potentials establish that (i) each redox process involves a one-electron oxidation and (ii) the oxidatively generated species are stable at ambient temperature for hours. Thus the electrochemically generated radical species can be studied by UV/vis and EPR spectroscopy.

Figure 2 (top) displays the electronic spectra of **1** and their electrochemically generated radical species $[\mathbf{1}]^{\bullet+}$ and $[\mathbf{1}]^{2\bullet2+}$. Solutions of **1** are colorless whereas those of the oxidized forms are green-brown. The spectrum of **1** displays two intense $\pi-\pi^*$ transitions of coordinated phenolates in the UV. Upon one-electron oxidation the typical intense $\pi-\pi^*$ transitions of a coordinated phenoxyl ligand are observed in the visible at 405 and 423 nm and, in addition, a weaker band at 549 nm (Table 3). Further oxidation to $[\mathbf{1}]^{2\bullet2+}$ changes the position of these bands only marginally but their intensities are twice as large. This is an indication that the phenolate and the phenoxyl in $[\mathbf{1}]^{\bullet+}$ and the two phenoxyls in $[\mathbf{1}]^{2\bullet2+}$ are electronically only weakly coupled.

Table 3. Electronic Spectra of Complexes[a])

complex	λ_{max}, nm (ϵ, L mol^{-1} cm^{-1})
1	253 (1.5×10^4), 316 (8.8×10^3)
$[\mathbf{1}]^{\bullet+}$	245 (9.9×10^3), 307 (1.8×10^4), 339 sh (6.1×10^3), 405 sh (5.4×10^3), 423 (6.6×10^3), 549 (160)
$[\mathbf{1}]^{2\bullet2+}$	238 (7.1×10^3), 310 (2.2×10^4), 332 sh (1.7×10^4), 408 sh (1.05×10^4), 429 (1.34×10^4), 562 (390)
2	252 (1.45×10^4), 314 (1.2×10^4), 458 (1.45×10^3), 698 (210)
$[\mathbf{2}]^{\bullet+}$	244 (1.0×10^4), 309 (1.8×10^4), 418 (5.4×10^3), 530 (2.3×10^3)
$[\mathbf{2}]^{2\bullet2+}$	237 (7.0×10^3), 319 (2.4×10^4), 431 (1.5×10^4), 485 (3.5×10^3)
3	235 (1.2×10^4), 296 (7.5×10^3), 312 (7.3×10^3)
$[\mathbf{3}]^{\bullet2+}$	312 (1.5×10^4), 413 sh (6.8×10^3), 431 (8.5×10^3), 535 (1.2×10^3)

[a] Measured in CH_2Cl_2 solution (0.10 M $[TBA]PF_6$) at 298 K; the phenoxyl radical species were generated electrochemically by controlled potential coulometry.

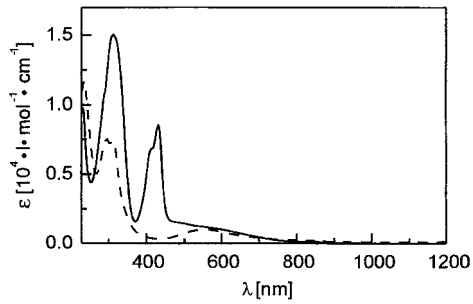

Figure 3. Electronic spectra of **3** (- - -) and its monooxidized form $[\mathbf{3}]^{\bullet2+}$ (—) in CH_2Cl_2 solution (0.10 M $[TBA]PF_6$) at 298 K.

Figure 2 (bottom) exhibits the electronic spectra of **2** and their electrochemically oxidized analogues $[\mathbf{2}]^{\bullet+}$ and $[\mathbf{2}]^{2\bullet2+}$. The spectrum of **2** is typical for square-based pyramidal phenolato copper(II) complexes. Two intense $\pi-\pi^*$ transitions of the phenolates in the UV, a band at 460 nm which has $O_{phenolate} \rightarrow Cu^{II}$ charge-transfer character and a weak d−d transition at ~700 nm, are observed. As observed above, upon one-electron oxidation the intense phenoxyl $\pi-\pi^*$ transition at 418 nm and an intense band in the visible at 530 nm are dominating the spectrum. In the spectrum of $[\mathbf{2}]^{2\bullet2+}$ the $\pi-\pi^*$ phenoxyl transition is split into two components at 431 and 485 nm. A very broad and intense absorption is observed in the visible.

Figure 3 shows the spectra of the protonated species **3** and $[\mathbf{3}]^{\bullet2+}$ where the latter species contains a phenoxyl and a phenol ligand. Interestingly, the intensity of the phenoxyl $\pi-\pi^*$ transition in $[\mathbf{3}]^{\bullet2+}$ is about twice as large as the corresponding transition of $[\mathbf{2}]^{\bullet+}$. For the broad absorption in the visible the opposite is true. This could point to a delocalization of the unpaired electron of the phenoxyl as depicted by the two resonance structures A and B for $[\mathbf{2}]^{\bullet+}$ shown in Scheme 2. In $[\mathbf{3}]^{\bullet2+}$ this is not possible. A similar interpretation has been given by Whittaker et al. for the spectrum of the active form of galactose oxidase, and we have shown this previously for the model complexes $[Cu^{II}(L^3H)]^{\bullet+}$ and $[Cu^{II}(L^3H_2)]^{\bullet2+}$.[3,15]

EPR Spectroscopy. X-band EPR spectra of frozen CH_2Cl_2 solutions of **2** and **3** at 40 K display axial or rhombic $S =$

(15) McGlashen, M. L.; Eads, D. D.; Spiro, T. G.; Whittaker, J. W. *J. Phys. Chem.* **1995**, *99*, 4918.

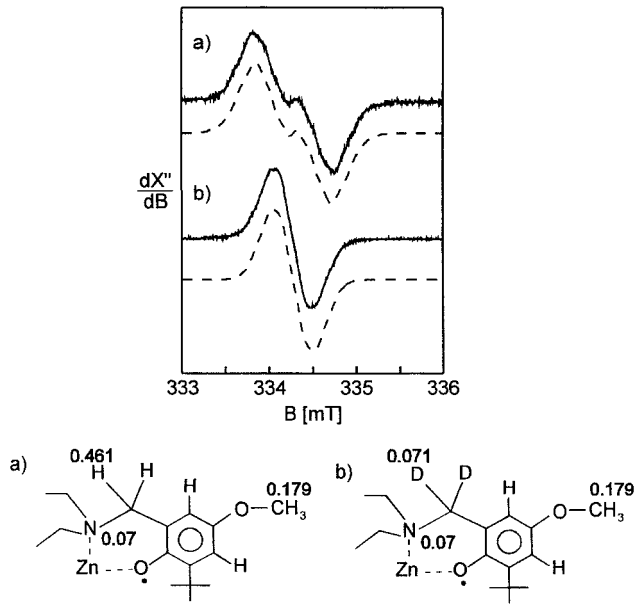

Figure 4. X-band EPR spectra of (a) $[\mathbf{1}]^{\bullet+}$ and (b) $[\mathbf{1}\text{-}d_2]^{\bullet+}$ in CH_2Cl_2 solution (0.10 M $[TBA]PF_6$) at 298 K (conditions: frequency, 9.4571 GHz; power, 1.0 mW; modulation amplitude, 0.02 mT). The hyperfine coupling constants from the fits (dotted lines) are given in mT.

Scheme 2. Possible Resonance Structures for a cis-(Phenolato)phenoxylcopper(II) Species

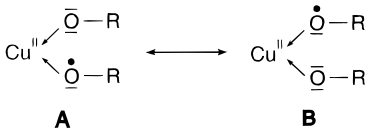

$^1/_2$ signals with copper-hyperfine splitting. They are typical for square-based pyramidal Cu^{II} complexes. The spectra and their simulations are shown in the Supporting Information. The following parameters were obtained from fits. **2**: $g_x = 2.051$, $g_y = 2.052$, $g_z = 2.243$; $A_x = A_y = 18 \times 10^{-4}$ cm^{-1}; $A_z = 177 \times 10^{-4}$ cm^{-1}. **3:** $g_x = 2.06$, $g_y = 2.07$, $g_z = 2.23$; $A_x = A_y = 10 \times 10^{-4}$ cm^{-1}; $A_z = 155 \times 10^{-4}$ cm^{-1}. These values closely resemble those reported for similar model compounds and the inactive form of galactose oxidase.[1−8]

The X-band EPR spectrum of $[\mathbf{1}]^{\bullet+}$ in CH_2Cl_2 solution (0.10 $[TBA]PF_6$) at 298 K is shown in Figure 4. A broad hyperfine-split, isotropic $S = {}^1/_2$ signal at $g = 2.002$ has been observed. We have also recorded the spectrum of the selectively deuterium labeled compound $[\mathbf{1}\text{-}d_2]^{\bullet+}$ (benzyl group) which clearly establishes a large hyperfine coupling to one of the benzyl protons ($a_H/a_D \sim 6.5$). Thus the benzyl protons are diastereotopic in the phenoxyl species which demonstrates that the six-membered chelate ring $\overline{Zn-O_{phenoxyl}-C-C-C-N}$ persists in the radical state and is conformationally rigid. Hyperfine coupling to three protons of one methoxy groups of the phenoxyl and a weaker coupling to the neighboring amine nitrogen simulate the spectra satisfactorily. Other couplings are smaller and are not resolved within the Gaussian line width of $\Delta\nu_{1/2} = 0.11$ mT. The spectra show that the phenoxyl radical in $[\mathbf{1}]^{\bullet+}$ is localized at one phenyl ring; no delocalization involving the coordinated phenolate is observed. This result is in excellent agreement with the electronic spectra as discussed above. The X-band EPR spectrum of $[\mathbf{1}]^{\bullet+}$ in frozen CH_2Cl_2 solution at 10 K consists of a single isotropic signal at $g = 2.002$ where the hyperfine splitting is not resolved.

In contrast, the EPR spectrum of the electrochemically generated diradical $[\mathbf{1}]^{2\bullet2+}$ in frozen solution (0.5 mM in CH_2Cl_2, 0.1 M $[TBA]PF_6$) shows a symmetric pattern of five lines centered at $g = 2$ with about 30 mT overall splitting and a weak narrow half-field signal at $g = 4$. Figure 5 displays the spectrum recorded at 30 K (bottom) together with the numerically integrated trace (top) and the half-field derivative signal (bottom inset). Simulations of the experimental data are shown as thin solid and dashed lines labeled sim, a, b, and c, respectively.

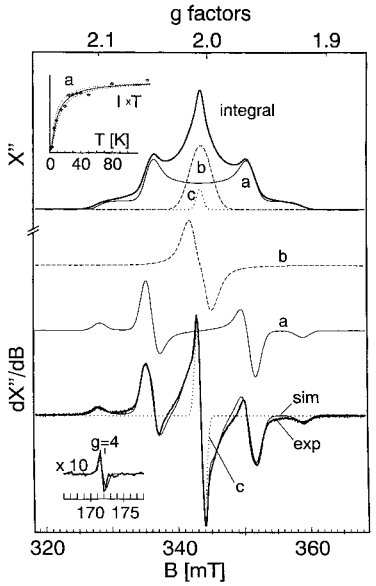

Figure 5. X-band EPR spectrum of electrochemically generated $[\mathbf{1}]^{2\bullet2+}$ in CH_2Cl_2 solution (0.5 mM, 0.10 M $[TBA]PF_6$) at 30 K. Bottom: Experimental derivative spectrum (conditions: microwave frequency, 9.6443 GHz; power, 0.8 μW, modulation, 0.8 mT, 100 kHz) and spin-Hamiltonian simulations using eq 4 for $S = 1$. Top: Numerically integrated experimental spectrum with corresponding simulations. Bottom inset: "$\Delta m = 2$" transitions at $g = 4$ with simulation (only subspectrum a contributes). Top inset: Temperature variation of the integral intensity of subspectrum a measured with 200 nW power. The solid line is a fit with a Boltzmann function[16] for a singlet−triplet gap $\Delta = 6.4$ cm^{-1}; the dashed lines indicate the error range $\Delta \pm 2$ cm^{-1}.

The spectrum is virtually independent of the sample concentration in the range 0.05−1.5 mM and of the EPR frequencies 3.3−33.9 GHz (S-, X-, and Q-band), except for the expected attenuation of the half-field signal with increasing frequency (not shown). The dominating central line at $g = 2$, however, varied significantly in its intensity for different preparations. It also showed a saturation behavior different from that of the other resonances. The spectrum was therefore deconvoluted into different subspectra by simulations.

The major part of the spectrum can be assigned to spin triplet resonances which give rise to the symmetrical split-line pattern (a). Its contribution accounts for 71% of the integral intensity, which can be seen best in the (absorption) spectrum in the top of Figure 5. The presented simulation is obtained from a spin Hamiltonian calculation for an isolated spin triplet with axial zero-field splitting (ZFS), which arises from the combined effect of intramolecular exchange and spin−dipolar couplings of the diradical spins. From optimization of the simulation parameters we obtained for the ZFS $D = 0.014(1)$ cm^{-1} and $E/D = 0(0.01)$; the (isotropic) g factor is 2.0042, and the line shape is Gaussian with a frequency-constant width $\sigma = 2.6$ mT (fwhm at $g = 2$). The temperature dependence of subspectrum a in the range 3−125 K reveals an excited state for the spin triplet, as shown in the top inset of Figure 5. This means that the spins in the diradical $[\mathbf{1}]^{2\bullet2+}$ are antiferromagnetically exchange-coupled with a total spin singlet ground state. A fit of the intensity of

subspectrum a with the appropriate Boltzmann function[16] reveals a singlet−triplet gap of 6.4 cm^{-1} (top inset of Figure 5), according to an exchange coupling constant $J = -3.2$ cm^{-1}. Although this value is smaller than that for several other diradical complexes, it is much larger than the Zeeman splitting ($h\nu = 0.3$ cm^{-1} at X-band frequencies) as well as the ZFS of the triplet. In this regime, singlet and triplet states are well separated without significant level mixing and it is safe to treat the triplet as isolated state in the spin Hamiltonian calculations.[17,18] This justifies our simulation approach. Furthermore, it can be assumed that pseudodipolar contributions from anisotropic exchange interaction are negligible,[18] which means that the ZFS owes its origin exclusively to dipolar interactions. In terms of the traceless dipole coupling tensor $\mathbf{J^d}$, the obtained ZFS parameters in axial symmetry ($D = 0.014$ cm^{-1}, $E/D = 0$) correspond to a main component J^d_z of -0.02 cm^{-1}, obtained from the relation[18]

$$J^d_z = {}^4/_3 D \tag{2}$$

In a point−dipole model this value would be related to a dipole−dipole distance of $r = 5.6$ Å, due to the relation[19] in eq 3 (where μ_B has the numerical value 0.433 when J^d_z is in

$$J^d = -8\mu_B r^{-3} \tag{3}$$

$cm^{-1}$and r is given in Å). As this distance is much larger than the separation of the oxygen atoms of the phenolates (2.75 Å) in **1**, the radical spins are not "localized" on the phenoxyl oxygen atoms in $[\mathbf{1}]^{2\bullet 2+}$ (as expected). In a more sophisticated model based on the molecular structure of **1** it was possible to probe the spin density distribution on the phenoxyl groups in some detail. To this end we assumed that the overall structure and, in particular, the dihedral angle of 15.2° between the two phenol rings and the distance of 2.75 Å between the two phenolate oxygen atoms remain invariant upon two-electron oxidation. We calculated the tensor $\mathbf{J^d}$ from a sum of fractional point−dipole contributions where the "true" electron spin distribution is replaced by a number of point charges situated in the π-orbitals lobes of the phenoxyl ring system, 0.65 Å above and below the ring plane. Local densities of the unpaired electrons at the individual C and O atoms were taken from density functional calculations on p-$CH_3OC_6H_4O^\bullet$ by Wheeler and Quin.[20] From these values we obtain (in the principal axes system) $\mathbf{J^d} = (+0.013, +0.016, -0.029)$ cm^{-1} in good agreement with the experimental value $(+0.01, +0.01, -0.02)$ cm^{-1}. This indicates that coordination to Zn^{II} has only a minor influence on the spin density distribution of the phenoxyl radicals.

The additional subspectra b and c that we had to introduce in the EPR simulation for $[\mathbf{1}]^{2\bullet 2+}$ were obtained as follows. The "inner part" of the central line shown in Figure 5 (trace c) is a narrow $S = {}^1/_2$ spectrum with parameters taken from the spectrum of the monoradical $[\mathbf{1}]^{\bullet +}$ at the same conditions, $g_{x,y} = 2.0042$, $g_z = 2.0065$, and $\sigma = 1.25$ mT (fwhm, Gaussian). Thus, we assign this weak contribution to a residual (5%) contamination with monoradical species that cannot be avoided in the electrochemical generation of the diradical.

In total, however, the central line is so broad that it could not be satisfactorily simulated with a simple Gaussian or Lorentzian powder spectrum. This does not support the presence of another monoradical as possible explanation. Since the width of the line is not concentration dependent, another monoradical with intermolecular dipolar boadening is also ruled out as origin of the subspectrum. We therefore tried a simulation with the assumption of a different spin triplet species with weak ZFS. This approach gave a good result (trace b) when the parameters $D = 0.0024$ cm^{-1}, $E/D = 0$, $g = 2.005$, and $\sigma = 3.2$ mT were adopted (24% intensity). It is in accordance with this model that the temperature dependence of the species appears to be very similar to that of subspectrum a, which indicates an excited state also for this spectrum. However, we were not able to measure the putative exchange splitting with reasonable accuracy, because saturation effects at liquid-helium temperatures obscured the intensity measurements for this subspectrum. In summary, we tend to assign the spectrum to a modification of $[\mathbf{1}]^{2\bullet 2+}$, where either the central Zn^{2+} ion is six-coordinate, containing a coordinated water molecule, or one phenoxyl group is not coordinated to Zn^{2+} or the Zn ion is completely released. The then expected electronic effects and/or the larger intramolecular separation of the radicals might explain the weak dipole interaction and ZFS of this diradical species.

EPR investigations in X-, S-, and Q-band on the monoradicals $[Cu^{II}(L)]^{\bullet +}$ and $[Cu^{II}(LH)]^{\bullet 2+}$ in frozen CH_2Cl_2 solutions in the temperature range 4−70 K revealed that these species are difficult to detect or they are even EPR silent. In each case mainly a residual signal of **2** and **3** (<4%), respectively, was observed. For $[Cu^{II}(L)]^{\bullet +}$ at liquid-helium temperatures additional broad integer-spin resonances occurred at low fields. They could be reasonably simulated with $S_t = 1$ and an unusually large ZFS with $D = 0.32$ cm^{-1} and $E/D = 0.27$. A very large frequency-dependent line width $\sigma_v = 150$ mT (fwhm at $g = 2$) had to be used, which indicates considerable inhomogeneity and g-strain in the frozen solution (see Figure S2). Due to these broadening effects high-frequency measurements (Q-band) also did not yield resolved spectra. The triplet is certainly populated at temperatures 4−20 K, which means that the exchange interaction is ferromagnetic or, at most, weakly antiferromagnetic. Unfortunately, the low intensity of the broad derivative signals prevents reliable measurements of their temperature dependence. We therefore cannot establish experimentally whether the triplet is the spin ground state and how strong the exchange interaction is. It appears that the large ZFS of $[\mathbf{2}]^{\bullet +}$ is at the limit where spin triplets can be measured using conventional EPR. Therefore, the protonated complex $[Cu^{II}(LH)]^{\bullet 2+}$ might be EPR silent due to either of two mechanisms: (i) relatively strong antiferromagnetic exchange yielding an $S_t = 0$ ground state or (ii) prohibitively strong (and inhomogeneous) ZFS of an $S_t = 1$ ground state.

Bearing these results in mind, the observed X-band EPR spectrum of the diradical $[Cu^{II}(L)]^{2\bullet 2+}$ ($[\mathbf{2}]^{2\bullet 2+}$) in frozen CH_2Cl_2 solution at 8 K shown in Figure 6 (bottom) is surprising. In the temperature range 4−30 K a dominating, narrow Cu^{II} spectrum at $g \approx 2$ is observed, which is superimposed by two groups of weak signals in a broad field range at effective g factors close to 5 and 3. Numerical integration of the experimental derivative spectrum discloses the high intensity (>80%) of this shallow derivative contribution (Figure 6, top). A well-resolved 4-line hyperfine pattern at $g^{eff} = 5.1$ with coupling constant $A = 140 \times 10^{-4}$ cm^{-1} establishes that it represents a

(16) The product intensity times temperature was fitted with the function $I \cdot T = \text{const} \exp\{-\Delta/kT\}/(1 + 3\exp\{-\Delta/kT\})$, where I is the intensity of the EPR spectrum and T is the temperature in K.

(17) Pilbrow, J. R. *Transition Ion Electron Paramagnetic Resonance*; Clarendon Press: Oxford, U.K., 1990.
(18) Smith, T. D.; Pilbrow, J. R. *Coord. Chem. Rev.* **1974**, *13*, 173−278.
(19) Bencini, A.; Gatteschi, D. *EPR of Exchange Coupled Systems*; Springer-Verlag: Berlin, 1990.
(20) Quin, Y.; Wheeler, R. A. *J. Am. Chem. Soc.* **1995**, *117*, 6083.

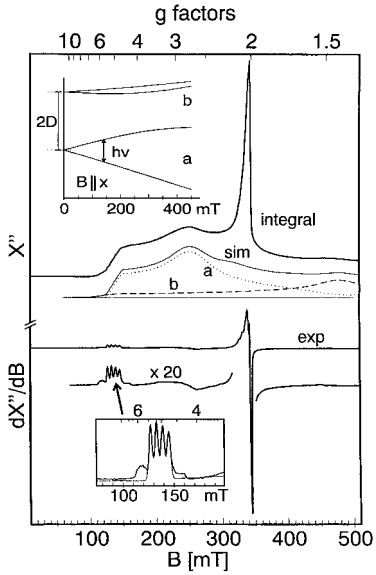

Figure 6. X-band EPR spectrum of $[\mathbf{2}]^{2\bullet 2+}$ in CH_2Cl_2 solution (0.5 mM, 0.10 M $[TBA]PF_6$) at 10 K. Top: Numerically integrated experimental spectrum (integral) and powder simulation (sim) obtained with the spin Hamiltonian (eq 4) for $S = {}^3/_2$ with $D = 0.4$ cm^{-1} and $E/D = 0.19$. The dotted and dashed lines labeled a and b show the individual subspectra from the $m_s =$ "$\pm{}^1/_2$" and the $m_s =$ "$\pm{}^3/_2$" Kramers doublets. Top inset: Example of the magnetic levels of the $S_t = {}^3/_2$ system, shown as a function of the applied field in molecular *x*-direction. The labels a and b denote the $m_s =$ "$\pm{}^1/_2$" and the $m_s =$ "$\pm{}^3/_2$" Kramers doublets, according to the depicted EPR subspectra in powder average.

Cu^{II} complex with a structure similar to that of [**2**] ($A_z = 177 \times 10^{-4}$ cm^{-1}). The effective *g* values close to $g^{eff} = 4$ indicate a high spin state. We show in the following that the signals originate from the $[\mathbf{2}]^{2\bullet 2+}$ diradical complex. *Ferromagnetic* exchange coupling of Cu^{II} and the coordinated phenoxyl radicals gives rise to a total spin $S_t = {}^3/_2$ ground state. This is unexpected since the other complexes with the same ligand, namely the Zn^{II} diradical complex $[\mathbf{1}]^{2\bullet 2+}$ and possibly the Cu^{II} monoradical $[\mathbf{2}]^{\bullet +}$, show *antiferrromagnetic* exchange.

Since the prominent narrow subspectrum in Figure 6 accounts for less than 20% of the total EPR intensity of the sample and, furthermore, since its parameters ($g_\perp = 2.12$, $g_\parallel = 2.01$, $A_\perp = 50 \times 10^{-4}$ cm^{-1}, simulation not shown) differ considerably from those of [**1**] or [**2**], we assign the narrow subspectrum to a contamination with deteriorated material. In particular, it cannot represent the excited $S_t = {}^1/_2$ states of the $[\mathbf{2}]^{2\bullet 2+}$ spin system because its relative contribution is too weak and temperature independent. We did not detect any direct influence from the excited spin states in the range 4−30 K. Above 30 K, however, drastic broadening of the low-field signals occurs, due to spin relaxation. If we attribute this to the onset of "Orbach"-type relaxation between $S_t = {}^3/_2$ and $S_t = {}^1/_2$ states, and if we take the onset temperature as a measure for the quartet-doublet energy gap Δ, we obtain a rough estimate for the exchange coupling constant. In the limit of "linear" topology with strong Cu^{II}−phenoxyl coupling (*J*) and negligible radical−radical coupling (*J*′) the spin quartet-doublet gap would be $\Delta = 3J$. Adopting $\Delta = kT$ with $T = 30$ K, one obtains $\Delta = 21$ cm^{-1} and, hence, $J \approx +7$ cm^{-1} as an estimate for the strength of the Cu^{II}−phenoxyl exchange interaction. More realistically, one has to assume that the energy gap of ground and excited states includes also a (negative) contribution from finite radical−radical interaction, which for the "isomorphous" Zn^{II} complex $[\mathbf{1}]^{2\bullet 2+}$ was −3.2 cm^{-1}. In this picture the $S_t = {}^3/_2$ ground state of $[\mathbf{2}]^{2\bullet 2+}$ is achieved by *ferromagnetic* coupling of Cu^{II} and each of the radicals, dominating the weaker *antiferromagnetic* radical−radical interaction.

The broad EPR spectrum of $[\mathbf{2}]^{2\bullet 2+}$ could be reasonably well simulated in the integrated representation (Figure 6, top) by using the appropriate spin Hamiltonain for $S_t = {}^3/_2$ (eq 4 in Experimental Section) with parameters $D = 0.4$ cm^{-1}, $E/D = 0.19$, and $g = 2$ (isotropic). For simplicity, the hyperfine coupling with $^{63/65}$Cu was considered only in first-order approximation. The lines were taken to be Gaussians with a frequency-dependent width[17] $\sigma_v = 10$ mT (fwhm at $g = 2$). A field- and angular-dependent part $\sigma_B = (50, 0, 50)$ mT was added to account for unresolved hyperfine splittings and *g*-strain effects. The result of the simulation is shown as solid line (sim) below the integrated spectrum in Figure 6. The level scheme of the $S_t = {}^3/_2$ multiplet with the corresponding ZFS parameters is depicted in the top inset of Figure 6 for one orientation selected from the powder distribution of molecules, namely for the field applied in *x*-direction.

In the simulations the *D* value had to be sufficiently large, so that the Kramers doublets are energetically separated and interdoublet transitions do not occur. At least in the measured field range such transitions were not observed in the X-band spectra. With $D = 0.4$ cm^{-1} the peak at $g^{eff} = 5.1$ and the absorption maximum at 2.9 originate from transitions in the $m_s =$ "$\pm{}^1/_2$" Kramers doublet for field orientations close to the molecular *y*- and *x*-directions, respectively. The $m_s =$ "$\pm{}^3/_2$" Kramers doublet yields only a very broad powder spectrum with a shallow maximum at $g^{eff} \approx 1.4$. This theoretically expected peak is experimentally not very pronounced, probably because of *g*-strain broadening. Additionally, the accuracy of numerical integration of the experimental spectrum is also not very high in such wide field ranges, due to possible baseline errors. An upper limit for *D* is obtained from the position and the shape of the $g^{eff}{}_z$ signals of the $m_s =$ "$\pm{}^1/_2$" Kramers doublet. In our case these resonances are considerably upfield shifted (beyond the measured field range) which is due to level mixing and repulsion by competing ZFS and Zeeman interaction at high fields. The finally obtained *D* value is surprisingly large, since none of the individual spins contributes with a single ion ZFS and the splitting of the quartet is solely due to dipolar coupling.[21] This shows the stronger dipolar interaction of Cu^{II} and coordinated phenoxyl radicals, compared to the radical−radical interaction of the Zn^{II} complex $[\mathbf{1}]^{2\bullet 2+}$, where *D* is only 0.014 cm^{-1} or compared to $D = 0.086$ cm^{-1} reported previously for another Cu^{II} phenoxyl complex with similar structure.[11] The same large ZFS, however, was found above also for the monoradical $[\mathbf{2}]^{\bullet +}$ ($D = 0.32$ cm^{-1}). Therefore, distinct differences can be assumed for the spin density distributions of these complexes.

Conclusion

In summary, the electrochemically generated radical complexes $[\mathbf{2}]^{\bullet +}$, $[\mathbf{2}]^{2\bullet 2+}$, and $[\mathbf{3}]^{\bullet +}$ exhibit spin ground states that are determined by weak ferromagnetic or antiferromagnetic exchange interaction of metal ion and coordinated radicals. Except for $[\mathbf{3}]^{\bullet +}$ this is shown from the EPR spectra of frozen solutions. The corresponding Zn^{II} diradical complex $[\mathbf{1}]^{2\bullet 2+}$ was used to probe separately that the (antiferromagnetic) radical−radical interaction is also weak. Accordingly, we can safely conclude that in the complex three-spin system of $[\mathbf{2}]^{2\bullet 2+}$ the S_t

(21) Anisotropic exchange is here neglected because the exchange interaction is weak.[18] For other Cu^{II} radical complexes it was previously considered (Bencini, A.; Benelli, C.; Gatteschi, D.; Zanchini, C. *J. Am. Chem. Soc.* **1984**, *106*, 5813 and references therein).

$= {}^3/_2$ ground-state results from prevailing *ferromagnetic* phenoxyl−Cu^{II} coupling.

In terms of the $Cu^{II}-O-C_{phenyl}$ bond angle α and the dihedral angle β between Cu *x*/*y*-plane and phenyl ring that we introduced in Scheme 1, the complexes are in line with all other five-coordinate copper(II) compounds containing 1,4,7-triazacyclononane-derived phenoxyl ligands reported to date.[1−8] These were found to be EPR-silent, supposedly due to antiferromagnetic exchange interaction.[11] However, for all of the compounds, the angles are throughout in the same range $\alpha = 127-130°$ and $\beta = 27-30°$. The fact that we now observe EPR spectra and weak ferromagnetic or antiferromagnetic exchange interactions in the present series means that their molecular structures induce a borderline situation where ferro- and antiferromagnetic contributions to the exchange interactions are very similar and almost cancel each other. Therefore, minor geometric or electronic variations might determine opposite signs of the composite coupling constant *J*, which essentially loose their physical meaning if $|J|$ is only a few wavenumbers. In this respect, it appears that only galactose oxidase represents a clear-cut case, since the coordinate tyrosyl ring is fixed by π-stacking interaction in the protein at $\alpha = 130°$, and $\beta = 75°$, which certainly allows substantial overlap of the magnetic orbitals and, hence, leads to strong antiferromagnetic exchange interaction and a well-isolated $S_t = 0$ ground state.

Experimental Section

1-Ethyl-4,7-bis(3-*tert*-butyl-5-methoxy-2-hydroxybenzyl)-1,4,7-triazacyclononane (H_2L). Paraformaldehyde (0.48 g, 16 mmol) was added to a solution of 1-ethyl-1,4,7-triazacyclononane (1.0 g, 6.4 mmol) in methanol (20 mL). After heating of the solution to reflux for 1 h, 2-*tert*-butyl-4-methoxyphenol (2.8 g, 15.4 mmol) was added and heating to reflux was continued for 23 h. The solvent was removed by rotary evaporation, and the residue was dissolved in *n*-hexane. The colorless ligand H_2L precipitated from this solution at 0 °C within 2−3 d. Yield: 3.0 g (87%). Anal. Calcd for $C_{32}H_{51}N_3O_4$: C, 70.94; H, 9.49; N, 7.76. Found: C, 70.97; H, 9.54; N, 7.78. ^{1}H NMR (400 MHz, $CDCl_3$): $\delta = 1.01$ (t, 3H), 1.40 (s, 9H), 2.56 (m, 4H), 2.56 (q, 2H), 2.72 (m, 4H), 2.97 (s, 4H), 3.69 (s, 2H), 3.71 (s, 2H), 6.34 (d, $J = 2.70$ Hz, 1H), 6.78 (d, $J = 2.70$ Hz, 1H) ppm. ^{13}C{^{1}H} NMR (100 MHz, $CDCl_3$): $\delta = 12.8$, 29.4, 34.8, 52.5, 55.4, 55.6, 55.8, 62.9, 111.2, 112.7, 123.7, 137.9, 150.5, 151.7 ppm. The synthesis of the deuterium-labeled compound (L^2-d_4) was performed by using the above recipe. Deuterioparaformaldehyde was used as starting material, and CH_3OD, as solvent. The ^{1}H NMR spectrum is the same as above but lacks the signals at $\delta = 3.69$ and 3.71 ppm of the benzylic protons.

[Zn^{II}(L)]·H_2O (1). A solution of H_2L (541 mg, 1.0 mmol) and $Zn(BF_4)_2 \cdot 4H_2O$ (239 mg, 1.0 mmol) in methanol (40 mL), to which $K[OC(CH_3)_3]$ (336 mg, 3.0 mmol) had been added, was heated to reflux for 2 h. After filtration of the hot solution colorless crystals of **1** precipitated (410 mg, 67%). Anal. Calcd for $C_{32}H_{51}N_3O_5Zn$: C, 61.68; H, 8.25; N, 6.74. Found: C, 61.51; H, 8.27; N, 6.76. ^{1}H NMR (400 MHz, $CDCl_3$): $\delta = 0.87$ (t, 3H), 1.49 (s, 18H), 2.43 (m, 4H), 2.46 (q, 2H), 2.77 (m, 6H), 3.03 (m, 2H), 3.33 (d, $J = 9.34$ Hz, 2H), 3.71 (s, 6H), 4.56 (d, $J = 9.34$ Hz, 2H), 6.40 (d, $J = 2.50$ Hz, 2H), 6.85 (d, $J = 2.50$ Hz, 2H) ppm. ^{13}C{^{1}H} (100 MHz, $CDCl_3$): $\delta = 11.2$, 29.8, 35.4, 49.3, 50.7, 52.2, 52.3, 52.7, 53.4, 56.0, 63.1, 113.2, 114.1, 120.9, 139.9, 147.2, 161.1 ppm.

[Cu^{II}(L)]·0.5 CH_2Cl_2 (2). A solution of H_2L (541 mg, 1.0 mmol) and CuCl (99 mg, 1.0 mmol) in methanol (40 mL), to which $K[OC(CH_3)_3]$ (336 mg, 3.0 mmol) had been added, was heated to reflux in the presence of air for 2 h whereupon the color changed to brownish green. After filtration and addition of CH_2Cl_2 (10 mL) green brown crystals precipitated within a few minutes (430 mg; 66%). Complex **2** displays a temperature-independent magnetic moment of 1.83 μ_B ($g = 2.12$) in the temperature range 2−290 K (SQUID). There is no detectable spin coupling in the dimer. Anal. Calcd for $C_{32.5}H_{50}N_3O_4ClCu$: C, 60.35; H, 7.95; N, 6.50. Found: C, 60.24; H, 7.91; N, 6.42.

Table 4. Crystallographic Data for **1**·H_2O, and **2**·0.5CH_2Cl_2

	1·H_2O	**2**·0.5 CH_2Cl_2
empirical formula	$C_{32}H_{51}N_3O_5Zn$	$C_{32.5}H_{50}ClCuN_3O_4$
fw	623.13	645.74
space group	*Pbca*	*C*2/*c*
a, Å	21.100(4)	14.447(2)
b, Å	10.267(2)	25.522(4)
c, Å	28.896(6)	17.296(3)
β, deg	90	98.96(2)
V, Å	6260(2)	6300(2)
Z	8	8
T, K	100(2)	100(2)
ρ_{calcd}, g cm^{-3}	1.322	1.362
μ(Mo Kα), cm^{-1}	8.28	8.19
reflns collcd	57292	37671
unique reflns/$I > 2\sigma(I)$	12 439/9487	5903/4269
no. of params	378	388
$2\Theta_{max}$, deg	68.3	55.0
R1[a] [$I > 2\sigma(I)$]	0.0431	0.0383
wR2[b] [$I > 2\sigma(I)$]	0.0830	0.0844

[a] $R1 = \sum||F_o| - |F_c||/\sum|F_o|$. [b] $wR2 = [\sum[w(F_o^2 - F_c^2)^2]/\sum[w(F_o^2)^2]]^{1/2}$, where $w = 1/\sigma^2(F_o^2) + (aP)^2 + bP$, $P = (F_o^2 + 2F_c^2)/3$.

[Cu(LH)](ClO$_4$) (3). When to the above reaction mixture after heating to reflux for 2 h was added a drop of concentrated $HClO_4$, a color change to deep violet was observed. Within a few hours at ambient temperature violet needle-shaped crystals precipitated (340 mg; 49%). Anal. Calcd for $C_{32}H_{50}N_3O_8ClCu$: C, 54.61; H, 7.16; N, 5.97. Found: C, 54.72; H, 7.05, N, 5.88. FAB MS(MNBA): *m*/*z* 604 [$Cu(LH)^+$].

X-ray Crystallographic Data Collection and Refinement of the Structures. A colorless single crystal of **1** and a dark brown crystal of **2** were transferred to glass capillaries and sealed under argon. **1** was mounted on a Siemens SMART CCD-detector diffractometer whereas **2** was measured on a Nonius Kappa-CCD diffractometer. Both setups were equipped with a cryogenic nitrogen cold stream. Graphite monochromated Mo Kα radiation ($\lambda = 0.710\,73$ Å) was used. Crystallographic data for the compounds are listed in Table 4. Intensity data were collected at −173(2) °C. The data were corrected for Lorentz and polarization effects but not for absorption due to small absorption coefficients. The Siemens ShelXTL[22] software package was used for solution, refinement, and artwork of the structures. Structures were solved and refined by direct methods and difference Fourier techniques. Neutral atom scattering factors were obtained from standard tables.[23] All non-hydrogen atoms were refined anisotropically. Hydrogen atoms were placed at calculated positions and refined as riding atoms with isotropic displacement parameters.

Hydrogen atoms of the water molecule in **1** were located from the difference map and isotropically refined without further restraints. The dichloromethane molecule in **2** was found to be disordered on two positions near a crystallographic 2-fold axis. It was readily refined with occupancy factors of 0.5 given to C, H, and Cl atoms.

Physical Measurements. Electronic spectra of the complexes and spectra of the spectroelectochemical investigations were recorded on a Perkin-Elmer Lambda 19 spectrometer (range: 220−1400 nm). Cyclic voltammograms, square-wave voltammograms, and coulometric experiments were performed on EG & G equipment (potentiostat/galvanostat model 273 A). X-band EPR spectra of complexes in solution at 298 K (CH_2Cl_2 solutions containing 0.10 M [TBA]PF_6) were measured on a Varian E-9 X-band spectrometer with 100 kHz modulation frequency at 298 K in a quartz cell ($d = 0.3$ mm). Low-temperature S-, X-, and Q-band measurements on frozen solutions were carried out on a Bruker ESP 300E spectrometer equipped with a NMR field probe (Bruker ER035M and a microwave frequency counter HP5352B and an Oxford Instruments ESR 910 helium flow cryostat with an ITC 503 temperature controller). The temperature stability was ±0.2 K, and the temperatue

(22) ShelXTL V.5, Siemens Analytical X-ray Instruments, Inc., 1994.
(23) *International Tables for X-ray Crystallography*; Kynoch Press: Birmingham, U.K., 1991.

gradient across the sample was estimated to be less than 0.5 K. Simulations of the monoradical EPR spectra recorded from fluid solutions at ambient temperature were simulated with the program by F. Neese.[24] Spin-Hamiltonian simulations of the low-temperature EPR spectra of the diradicals were performed with programs that were developed from the $S = {}^5/_2$ routines of Gaffney and Silverstone[25] with the specific resonance-search procedure based on a Newton−Raphson algorithm as described therein. The line widths were usually taken to be constant on a frequency axis;[17] additional angular dependent terms were only applied for the $S = {}^3/_2$ species $[\mathbf{2}]^{2\bullet 2+}$ to account for nonresolved hyperfine splittings and eventually *g*-strain effects. The line shapes were either Lorentzian or Gaussian. Hyperfine splitting terms were completely neglected for $[\mathbf{1}]^{2\bullet 2+}$; in the simulation of $[\mathbf{2}]^{2\bullet 2+}$ they were considered by first-order perturbation treatment. These simulations are based on the usual spin Hamiltonian

$$H = D\,[S_z^2 - S(S+1)/3 + (E/D)(S_x^2 - S_y^2)] + \mu_B \mathbf{B}\cdot g\cdot \mathbf{S} \quad (4)$$

where $S = 1$ or $S = {}^3/_2$ was the total spin of the ground-state triplet ($[\mathbf{1}]^{2\bullet 2+}$) or quartet ($[\mathbf{2}]^{2\bullet 2+}$) and D and E/D are the usual axial and rhombic zero-field parameters. All NMR spectra were recorded on a 400 MHz Bruker AMX series spectrometer.

Acknowledgment. We thank the Fonds der Chemischen Industrie for financial support and Dr. K. Hildenbrandt for EPR measurements.

Supporting Information Available: Figure S1, showing the EPR spectra of **2** and **3**, and Figure S2, showing that of $[\mathbf{2}]^{\bullet +}$, and tables of crystallographic and crystal structure refinement data, atom coordinates, bond lengths and angles, anisotropic thermal parameters, and calculated positional parameters of hydrogen atoms for **1** and **2**. This material is available free of charge via the Internet at http://pubs.acs.org.

IC990396J

(24) Neese, F. Diploma Thesis, University Konstanz/Germany, 1994.
(25) Gaffney, B. J.; Silverstone, H. J. Simulation of the EMR Spectra of High-Spin Iron in Proteins. In *Biological Magnetic Resonance*; Berliner, L. J., Reuben, J., Eds.; Plenum Press: New York, London, 1993; Vol. 13.